

Detection of electromagnetic multipoles by x-ray spectroscopies

S. Di Matteo,^{1,2} Y. Joly,³ and C. R. Natoli¹

¹Laboratori Nazionali di Frascati INFN, via E. Fermi 40 I-00044 Frascati (Roma), Italy

²Dipartimento di Fisica "E. Amaldi," Università di Roma 3, via della Vasca Navale 84, I-00146 Roma, Italy

³Laboratoire de Cristallographie, CNRS, BP166, F-38042 Grenoble Cedex 9, France

(Received 8 June 2005; revised manuscript received 15 July 2005; published 5 October 2005)

Following a brief discussion on electromagnetic multipole expansion, we provide a link between several multipole moments and the measurable quantities of some x-ray spectroscopies, like resonant x-ray scattering or dichroism in absorption. A general classification is given, accompanied by some specific examples and a geometrical interpretation of the axial toroidal (nonmagnetic) quadrupole, related to the x-ray natural circular dichroism. Finally, in order to provide a physical example for the detection of magnetic parity-odd multipoles, like the toroidal moment, we perform a numerical simulation for x-ray nonreciprocal directional dichroism, at the Fe *K* edge, in the polar ferrimagnet GaFeO₃. Our calculations describe quite well the reported experimental profile, with the correct order of magnitude for dichroism/absorption intensity ratio and a signal which is limited to pre-edge.

DOI: 10.1103/PhysRevB.72.144406

PACS number(s): 75.80.+q, 78.70.Dm, 78.70.Ck, 78.20.Ls

I. INTRODUCTION

Multipole expansion of electric and magnetic fields generated by fixed charges and permanent currents is a widely used tool to characterize the electromagnetic state of a physical system.¹ For example, for a charge distribution $\rho(\vec{x})$ in a given external potential field $\Phi(\vec{x})$, whose electrostatic energy is $W_E = \int d^3x \rho(\vec{x})\Phi(\vec{x})$, one can exploit the well-known expansion: $W_E = q\Phi(0) - \vec{d} \cdot \vec{E} - \frac{1}{6} \sum_{ij} Q_{ij} (\partial E_i / \partial x_j)(0) + \dots$. Here (0) is some properly chosen origin, and $\vec{E} = -\nabla\Phi$. Such an expansion shows how the external field couples with the various multipoles of the charge distribution: the potential with the charge q , the electric field with the dipole \vec{d} , the gradient of the field with the quadrupole $Q_{ij} \equiv 3x_i x_j - r^2 \delta_{ij}$, and so on. A similar expansion holds also for the vector potential. In this case there is no monopole term, of course, and the magnetic energy is: $W_M = \int d^3x \vec{J}(\vec{x}) \cdot \vec{A}(\vec{x})$. However, due to the vector character of the current density \vec{J} and the potential \vec{A} , it is often useful to decompose them, before exploiting the expansion, in a longitudinal (rotor-free) and a transversal (divergenceless) part: $\vec{J} = \vec{J}_{\parallel} + \vec{J}_{\perp}$. As $\nabla \cdot \vec{J} = \nabla \cdot \vec{J}_{\parallel} \equiv -\partial_t \rho$, then the longitudinal \vec{J}_{\parallel} is related to the time derivative of the charge multipoles. On the other side, the solenoidal field \vec{J}_{\perp} is characterized by two independent families of moments, and can be written, in the Helmholtz-Debye representation, as: $\vec{J}_{\perp} = \vec{l}\psi(\vec{x}) + \vec{\nabla} \times [\vec{l}\chi(\vec{x})]$, where \vec{l} is the orbital angular momentum and $\psi(\vec{x})$ and $\chi(\vec{x})$ are a scalar and pseudoscalar function, respectively. The first vector describes the toroidal currents (flowing along the parallels on a sphere), and the second the poloidal currents (flowing along the meridians on a torus). Toroidal currents are widely used, e.g., in the physics of electron plasma. Following Ref. 2, we define the magnetic multipoles of the two families in terms of the orbital angular momentum; when also spin quantities play a role, it is sufficient to consider the substitution $\vec{l} \rightarrow \vec{l} + g_s \vec{s}$, where g_s is the spin giromagnetic ratio. Then we have

- (a) Magnetic moment: $\vec{m} = (e/2m)\vec{l} = \mu_B \vec{l}$;
- (b) Magnetic quadrupole: $m_{ij} = \mu_B (x_i l_j + l_i x_j)$;
- (c) Magnetic (polar) toroidal moment: $\vec{t} = \oint (\vec{x} \times \vec{m}) d^3x$;
- (d) Magnetic toroidal quadrupole: $t_{ij} = x_i l_j + l_i x_j$.

Notice that the magnetic toroidal moment is known in high-energy physics as anapole.³ A simple geometrical image of \vec{t} is a closed circle of elementary magnets \vec{m} joined to each other. By analogy with this image, one can define a similar quantity,⁴ by replacing \vec{m} with the electric dipole \vec{d} . Then we get

- (e) Axial toroidal moment: $\vec{g} = \oint (\vec{x} \times \vec{d}) d^3x$;
- (f) Axial toroidal quadrupole: $g_{ij} = x_i g_j + g_i x_j$.

These moments are scalarly coupled with the corresponding fields in the following way: \vec{m} and m_{ij} couple, respectively, with the magnetic field \vec{B} and its gradient $\partial_i B_j$; magnetic toroidal moment \vec{t} and quadrupole t_{ij} couple, respectively, with the time-reversal (\hat{T}) odd and inversion (\hat{P}) odd vector $\vec{E} \times \vec{B}$ and its \hat{P} -even gradient $\partial_i (\vec{E} \times \vec{B})_j$; finally, axial toroidal moment \vec{g} and quadrupole g_{ij} couple with the \hat{T} -even and \hat{P} -even vector $\vec{E} \times \vec{B} (\vec{E} \cdot \vec{B})$ and its \hat{P} -odd gradient $\partial_i (\vec{E} \times \vec{B})_j (\vec{E} \cdot \vec{B})$. In order to have nonzero toroidal moments and quadrupoles, the symmetry of the crystal must be subject to special conditions: in fact, (c) is \hat{T} and \hat{P} -odd, (d) is \hat{T} -odd and \hat{P} -even, (e) is \hat{T} and \hat{P} -even, and (f) is \hat{T} -even and \hat{P} -odd. Remarkably, in a polarized system, the interaction of the dipole \vec{g} with the fields \vec{E}, \vec{B} is possible also at a lower order and in the absence of a net magnetization: the corresponding free-energy is $F \propto \vec{g} \cdot (\vec{D} \times \vec{E})$, where \vec{D} is the (local or global) polarization of the system.² The knowledge of electric and magnetic multipoles of both parities under space inversion and time reversal can be of great importance in order to understand the electromagnetic behavior of the material: the possibility to use any of these multipoles as an order parameter in phase transitions has been analyzed, e.g., in Ref. 2.

The aim of this paper is to show how it is possible to detect most of the previous multipoles by means of resonant

x-ray spectroscopies. In Sec. II we shall explicitly write the one-to-one correspondance of each multipole with the measurable quantities in resonant x-ray scattering (RXS) and dichroism in absorption. In particular, the results of x-ray natural circular dichroism⁵ (XNCD) is interpreted as a measure of the nonmagnetic toroidal quadrupole of the system, g_{ij} , contrary to what is presently believed.⁶ Finally, in Sec. III we perform a calculation to describe the results of a recent non-reciprocal dichroism experiment, called x-ray directional dichroism, in the polar ferrimagnet GaFeO₃.⁷ The physical quantities involved in such a dichroism are shown to be a mixture of magnetic quadrupole, toroidal magnetic moment and octupole, i.e., quantities resulting from dipole-quadrupole ($E1-E2$) interference which are parity and time-reversal odd.

II. MULTIPOLAR TERMS IN RXS AND ABSORPTION

Core resonant spectroscopies are described by the virtual processes that promote a core electron to some empty energy levels. They all depend on the transition matrix elements of matter-radiation interaction

$$M_{ng}^{i(o)}(j) = \langle \psi_n | \hat{O}^{i(o)} | \psi_g(j) \rangle, \quad (1)$$

where, in the x-ray regime, the operator \hat{O} is written through the multipolar expansion of the photon field up to electric dipole ($E1$) and quadrupole ($E2$) terms⁸

$$\hat{O}^{i(o)} = \vec{\epsilon}^{i(o)} \cdot \vec{r} \left(1 - \frac{1}{2} i \vec{k}^{i(o)} \cdot \vec{r} \right). \quad (2)$$

In Eq. (1), $\psi_g(j)$ is the core ground state centered around the j th atom and ψ_n the photoexcited state, whereas in Eq. (2), \vec{r} is the electron position measured from the absorbing ion, $\vec{\epsilon}^{i(o)}$ is the polarization of the incoming (outgoing) photon and $\vec{k}^{i(o)}$ its corresponding wave vector. In RXS the global process of photon absorption, virtual photoelectron excitation and photon re-emission, is coherent throughout the crystal, thus giving rise to the usual Bragg diffraction condition

$$F = \sum_j e^{i\vec{Q} \cdot \vec{R}_j} (f_{0j} + f'_j + i f''_j). \quad (3)$$

Here \vec{R}_j stands for the position of the scattering ion j , \vec{Q} is the diffraction vector and f_0 is the usual Thomson factor. The resonant part, $f'_j + i f''_j \equiv f_j$, is the anomalous atomic scattering factor, given by the expression⁹

$$f_j(\omega) = \frac{m_e}{\hbar^2 \hbar \omega} \sum_n \frac{(E_n - E_g)^3 M_{ng}^{o*}(j) M_{ng}^i(j)}{\hbar \omega - (E_n - E_g) - i \frac{\Gamma_n}{2}}, \quad (4)$$

where $\hbar \omega$ is the photon energy, m_e is the electron mass, E_g is the ground state energy, and E_n and Γ_n are the energy and inverse lifetime of the excited states. The sum is extended over all the excited states of the system.

The connection with x-ray near edge absorption (XANES) is straightforward, as its cross-section σ simply corresponds to the imaginary part of $f_j(\omega)$ when $\hat{O}^o = \hat{O}^i$ (forward scattering)

TABLE I. Parity and time-reversal symmetries of $F_q^{(p)}$ tensors.

Tensor	\hat{T}	\hat{P}	Multipole
$F^{(0)}(E1-E1)$	+	+	Electric charge
$F^{(1)}(E1-E1)$	-	+	Magnetic dipole
$F^{(2)}(E1-E1)$	+	+	Electric quadrupole
$F^{(1+)}(E1-E2)$	+	-	Electric dipole
$F^{(2+)}(E1-E2)$	+	-	\vec{g} quadrupole
$F^{(3+)}(E1-E2)$	+	-	Electric octupole
$F^{(1-)}(E1-E2)$	-	-	Polar toroidal dipole
$F^{(2-)}(E1-E2)$	-	-	Magnetic quadrupole
$F^{(3-)}(E1-E2)$	-	-	Polar toroidal octupole
$F^{(3)}(E2-E2)$	-	+	Magnetic octupole
$F^{(4)}(E2-E2)$	+	+	Electric hexadecapole

$$\sigma = -4\pi \cdot 10^{22} \frac{a_0^2 \alpha^3 m_e c^2}{\hbar \omega} f'' \quad (5)$$

Here a_0 is the Bohr radius, α is the fine structure constant, c is the speed of light and the prefactors are such that σ is in Mbarn when f'' is in units of the classical electron radius, $r_0 \approx 2.82 \times 10^{-15}$ m.

The matrix element in Eq. (1) depends only on the electronic part of the operator \hat{O} , so that the radiation parameters $\hat{\epsilon}$ and \vec{k} can be factorized out. It is then possible to demonstrate^{10,11} that the RXS amplitude, Eq. (4), as well as XANES cross section, Eq. (5), can be expressed as scalar product of two irreducible tensors, $f_j(\omega) = \sum_{p,q} (-)^q T_q^{(p)} F_{-q}^{(p)}(j; \omega)$, where $T_q^{(p)}$ depends only on the incident and scattered polarization and wave vectors, while $F_q^{(p)} \times(j; \omega)$ represents the properties of the system under study. It is well known from the literature (see, e.g., Refs. 12–14, or Ref. 15, for a treatment in cartesian basis) that the rank p of these irreducible tensors depends on the order of the multipoles in the electromagnetic field expansion, Eq. (2): for example, in the $E1-E1$ channel $p=0, 1, 2$, in the $E1-E2$ channel $p=1, 2, 3$ and in the $E2-E2$ channel $p=0, 1, 2, 3, 4$. Moreover, for each p , $F_q^{(p)}(j; \omega)$ is related to a specific term of the multipolar expansion of the system, according to Table I.

For $p=0, 1, 2$, $E1-E1$ and $E2-E2$ tensors represent the same physical quantities, though referred to states with different angular momentum. The identification illustrated in the table is dictated by the unique properties under time reversal and parity reflections of $F^{(p)}$ tensors on one side and multipole terms on the other. In fact, for any given tensor rank $p=1, 2, 3, 4$, there is just one electromagnetic multipole of the same rank ($1 \rightarrow$ dipole, $2 \rightarrow$ quadrupole, $3 \rightarrow$ octupole, $4 \rightarrow$ hexadecapole) with the same \hat{T} and \hat{P} properties. Notice that \hat{P} -odd $E1-E2$ tensors have both \hat{T} -odd ($-$) and \hat{T} -even ($+$) terms for any p ,¹⁴ while \hat{P} -even tensors (both $E1-E1$ and $E2-E2$) are \hat{T} -odd if of odd rank and \hat{T} -even if of even rank.

As each $F^{(p)}$ is scalarly related to a corresponding $T^{(p)}$, they have the same \hat{T} and \hat{P} properties. For example, in the $E1-E1$ or $E1-E2$ channels, $T^{(0)} \equiv \hat{\epsilon}^{o*} \cdot \hat{\epsilon}^i$ is a scalar and $T^{(1)} \equiv \hat{\epsilon}^{o*} \times \hat{\epsilon}^i$ is a \hat{T} -odd and \hat{P} -even vector. Analogously, in the $E1-E2$ channel, the previous quantities combine with the two \hat{P} -odd vectors $\vec{k}^i + \vec{k}^o$, which is \hat{T} -odd, and $\vec{k}^i - \vec{k}^o$, which is \hat{T} -even (see, e.g., Ref. 16 for a more complete analysis of this case).

Up to now, we have deliberately avoided the question of whether the local density of the tensors probed by this spectroscopy has anything to do with the properties of the ground state, which we are interested in. At first sight, the presence of the core hole in the final state would be prone to give a negative answer to this question, and yet, the wide success of sum rules for magnetic circular dichroism¹⁷ seems to prove the contrary. Moreover, in Ref. 14 in the framework of multiple scattering theory, it was demonstrated that these spectroscopies are sensitive to the expectation values of some tensor operators in the scattering states at the energy of the measurement, so that, by integrating over a specific edge, sum rules can be recovered.¹⁸ Thus, in the following we assume that we may refer to the values of the multipoles in the ground state.

The sum rule related to K edge magnetic circular dichroism is well known:¹⁷ in the $E1-E1$ channel, the dichroic signal is proportional to the orbital magnetic moment \vec{l} projected along the photon wave vector. Similarly, in the $E1-E2$ channel, XNCD was found to be sensitive to the mean value of the tensor $F^{(2+)}(E1-E2)$.⁵ It is interesting to note that this latter has been interpreted in the past^{6,11,16} as the expectation value of the physical quantity $\langle l_z t_z \rangle$, while from the previous table it comes out that this term measures the quadrupole of \vec{g} , which is time reversal even and parity-odd. Quantitatively, the former identification is not incorrect, as the expectation values of the operators $\langle l_z t_z \rangle$ and $\langle r_z g_z \rangle$ between states with $\Delta l = \pm 1$ are proportional to each other. However, from the physical point of view it seems rather singular that a non-magnetic quantity like XNCD be related to the expectation value of two magnetic terms like \vec{l} and \vec{l} . It is now clear that $l_z t_z$ is nothing but an effective operator representing the \vec{g} quadrupole when averaged between states differing by one unit of angular momentum. Therefore, it is the \vec{g} quadrupole that measures the rotatory power in XNCD and RXS spectroscopies.

A simple geometrical model that may help in the visualization of such a term can be constructed as follows. Consider any local structure with \hat{C}_3 symmetry, like V^{3+} ions in corundum V_2O_3 or I^{3+} ions in α - $LiIO_3$. Such structures can be seen from the threefold axis as superpositions of a trigonal distortion (D_{3d} local symmetry) and a relative threefold twisting of the oxygens ‘‘above’’ and ‘‘below’’ the cation, as shown in Fig. 1. In particular, Fig. 1(a) represents the untwisted situation, where the local symmetry is not lower than C_{3v} and no local $F^{(2+)}(E1-E2)$ term is allowed, as forbidden by the vertical mirror plane (see, e.g., Ref. 11). In Fig. 1(b), the arrows show the local displacement of the oxygens following a rotation about the (111) axis, which reduces the symmetry to C_3 : if, in first approximation, we consider the d

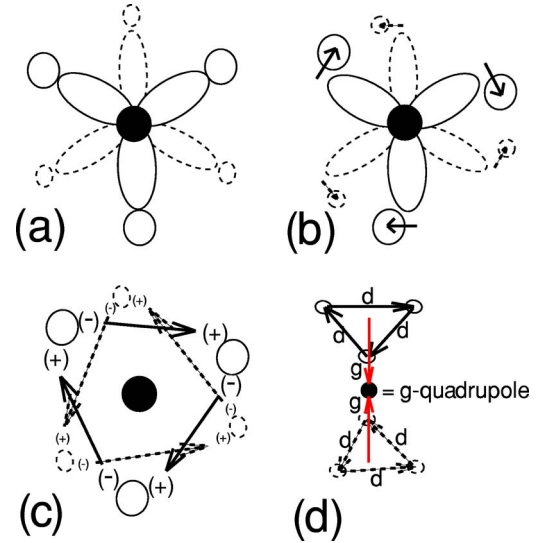


FIG. 1. (Color online) Schematic description of the formation of the g quadrupole. The local structure of corundum V_2O_3 is considered. The mechanism is explained in the text. The full circle indicates the V ion and the empty ones represent the oxygens. The (111) direction is perpendicular to the plane of the figure in (a), (b), and (c) and p -like orbitals are depicted in (a) and (b). Black arrows in (c) and (d) represent electric dipoles. Dashed objects lie below the V-ion plane.

orbitals as frozen, this induces a local polarization around the oxygens as shown by the charge positions in Fig. 1(c). This orbital polarization is in turn equivalent to the electric dipole configuration, drawn in Figs. 1(c) and 1(d), with a net rotation, oppositely oriented above and below the cation ion. As depicted in Fig. 1(d) such a configuration is equivalent to a couple of \vec{g} dipoles with opposite direction, in this way creating a quadrupole g_{ij} . Notice that when we relax the approximation of frozen orbitals, only an actual calculation can tell us whether the polarization still persists or not: *a posteriori* this is confirmed by the signals obtained through numerical *ab initio* simulations in Refs. 5 and 11.

These same quantities are detectable also by means of RXS, where the local transition amplitudes are added with a phase factor that can compensate the possible vanishing effect due to the global symmetry, as shown in Ref. 11 for the quadrupole of \vec{g} in the corundum phase of V_2O_3 and, e.g., in Ref. 19 for the magnetic moment in the antiferromagnetic insulating phase of V_2O_3 .

Thus, simply on the basis of their \hat{P} and \hat{T} properties shown in Table I, it follows that three of the four basic vectors (\vec{d} , \vec{m} , and \vec{l}) are detectable, while \vec{g} is not, as there is no rank-one tensor which is \hat{P} and \hat{T} -even. Similarly, it is not possible to detect with these techniques the magnetic toroidal quadrupole t_{ij} , as there is no rank-two tensor which is \hat{P} -even and \hat{T} -odd.

In conclusion, x-ray spectroscopies allow us to gain information about the following set of electromagnetic multipoles (the first five are parity-even, $E1-E1$ or $E2-E2$, the latter parity-odd, $E1-E2$):

(1) Charge, expressed by $F^{(0)}$. This is usually the stron-

gest contribution in both XANES and RXS. This term allows us to prove (or disprove) the so-called charge ordering through forbidden diffraction-peaks analysis (see, e.g., Ref. 20). In fact, any modification of the atomic charge implies a core level shift, and the measure of the energy shift of the threshold allows us to obtain the total valence charge with a good resolution.

(2) Magnetic moments [i.e., $F^{(1)}(E1-E1)$] have been treated in a widespread context, due to the big success of the ‘‘Carra-Thole-van der Laan’’ sum-rules.¹⁷

(3) Electric quadrupole [$F^{(2)}(E1-E1)$] is the biggest non-magnetic anisotropic term, responsible, e.g., for structural linear dichroism, as well as, in RXS signals, for the anomalous Jahn-Teller and ‘‘orbital ordering’’ peaks in systems like manganites.²¹

(4) Magnetic octupole [$F^{(3)}(E2-E2)$] was invoked in Ref. 22 to explain the anomalous RXS signal in NpO_2 and was proved to give a contribution in the anomalous magnetic signal in V_2O_3 .^{19,23}

(5) Electric hexadecapole [$F^{(4)}(E2-E2)$] was detected in α -haematite by Finkelstein and collaborators, as explained in Ref. 10.

(6) Electric dipole [$F^{(1+)}(E1-E2)$] is observable by RXS in antiferroelectric materials, like ErGe_3 or VOMoO_4 .²⁴

(7) Nonmagnetic (axial) toroidal quadrupole, as discussed above, was found with XNCD in α - LiIO_3 ,⁵ and in V_2O_3 by means of RXS.¹¹

(8) Electric octupole [$F^{(3+)}(E1-E2)$] has been predicted in Ref. 16 for K_2CrO_4 on the basis of symmetry arguments.

(9)–(10)–(11) Finally, magnetic toroidal moment [$F^{(1-)}(E1-E2)$] and octupole [$F^{(3-)}(E1-E2)$], together with magnetic quadrupole [$F^{(2-)}(E1-E2)$] have been found in the anomalous magnetic signal of V_2O_3 .¹⁹ Unfortunately, in this latter case all three terms were entangled with the magnetic octupole of $E2-E2$ origin, and it was not clear how to separate one from the other. The possibility of disentangling the three $E1-E2$ contribution has been demonstrated in Ref. 25 for $\text{Li}_2\text{VOSiO}_4$, where it was even shown how to extract each single term separately, by means of a series of azimuthal scans. However, this was just a theoretical prediction, not yet confirmed by an experiment. Of course, a much more cogent test to demonstrate the detectability of such quantities is represented by a convergent description of theory and experiment. Such an experiment has already been performed with a dichroic technique in absorption,^{7,27} and in the next section we shall provide its quantitative interpretation in terms of the three time-reversal and parity-odd quantities $F^{(1-)}(E1-E2)$, $F^{(2-)}(E1-E2)$, and $F^{(3-)}(E1-E2)$.

III. X-RAY NONRECIPROCAL DIRECTIONAL DICHROISM IN GaFeO_3 : ANALYTICAL AND NUMERICAL CALCULATIONS

GaFeO_3 is a piezoelectric crystal which was synthesized by Remeika more than 40 years ago.²⁷ Below about $T_c \approx 200$ K,²⁸ it also shows a spontaneous magnetization, with magnetic Shubnikov group $m'2'm$ which is characterized by an off-diagonal magnetoelectric susceptibility. A very large linear magnetoelectric effect was reported by Rado.²⁹ The

presence of both symmetric and antisymmetric parts in the magnetoelectric susceptibility tensor makes possible the detection of both nonreciprocal gyrotropy and magnetochiral effects through x-ray dichroism in absorption (see, e.g., Refs. 14 and 30). This possibility was realized in Ref. 7, in which a beautiful experiment was performed under the name of x-ray nonreciprocal directional dichroism (XNDD) whereby a time-reversal and parity-odd signal was detected. Even though we basically agree with the general interpretation given by the authors of Ref. 7 itself, their analysis is just semiquantitative and here we are able to provide a more comprehensive description of the experiment, which can frame the measured signal within the global picture described above. The aim of this subsection is to relate the XNDD signal to the dipole-quadrupole magnetic tensors $F^{(i-)}(E1-E2)$ ($i=1,2,3$) introduced above, discuss the physical meaning of each term, and substantiate the description by calculating the XNDD through an *ab initio* numerical code.²⁶

If we consider the crystal and magnetic structure given in Ref. 31, the total absorption signal at iron K edge is obtained as the average over the four Fe absorption sites in the unit cell, $\sigma \equiv \sum_{j=1,4} \sigma^{(j)}$, where $\sigma^{(j)}$ [Eq. (5)], can be expressed as

$$\sigma^{(j)} = 4\pi^2 \alpha \hbar \omega \sum_n |\langle \psi_n^{(j)} | \hat{O} | \psi_g^{(j)} \rangle|^2 \delta[\hbar\omega - (E_n - E_g)] \quad (6)$$

According to Refs. 7 and 31, the unit cell is orthorhombic, with an electric polarization along the screw b axis, and a net magnetization, below T_c , along the c axis. In the experiment performed in Ref. 7 four absorption spectra were measured, all with the x-ray wave vector directed along the a axis: in two cases the electric polarization was directed along the c axis, and in two cases along the b axis. For each of these two subcases, the magnetic moment was selected to be either parallel or antiparallel to the easy c axis, by means of an applied external magnetic field. We label them as $\sigma_c(H^+)$, $\sigma_c(H^-)$, $\sigma_b(H^+)$, $\sigma_b(H^-)$. The two measured dichroic spectra are then defined as: $\sigma_c \equiv \sigma_c(H^+) - \sigma_c(H^-)$, and $\sigma_b \equiv \sigma_b(H^+) - \sigma_b(H^-)$.

Before discussing the calculated numerical spectra, shown in Fig. 2, we just push our analytical derivation as far as possible, in order to demonstrate that the only quantities involved in this kind of dichroism are the tensors $F^{(i-)}(E1-E2)$ ($i=1,2,3$). First of all, from the definition of σ_c and σ_b , it is clear that only magnetic terms can contribute to the dichroism, as the structural absorption is the same for both H^\pm configurations. This selects just \hat{T} -odd contributions. It is convenient to choose the reference frame xyz in such a way that the quantization axis z coincides with the direction of the x-ray beam (the a crystallographic direction, in the configuration of Ref. 7), while x is directed along the electric polarization (b axis) and y along the magnetic moment (c axis). Even though the usually chosen reference frame is the one with the z axis along the magnetization,⁷ the frame considered here has the advantage that tensor properties acquire their simplest form. In this frame the polarizations have components $\hat{\epsilon} = \hat{\epsilon}^* = (1, 0, 0)$ for σ_b dichroism and $\hat{\epsilon} = \hat{\epsilon}^* = (0, 1, 0)$ for σ_c dichroism. In both cases, parity-even magnetic terms of $E1-E1$ and $E2-E2$ origin do not contribute,

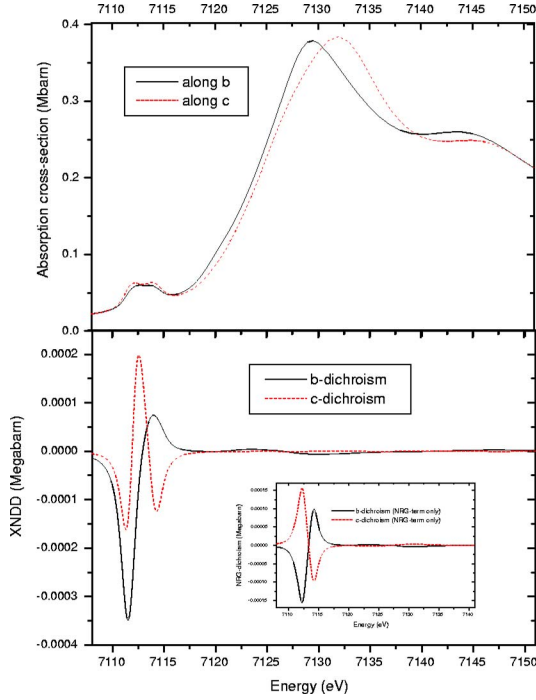


FIG. 2. (Color online) Theoretical simulation of absorption spectrum and XNDD. The inset shows the contribution of σ_{NRG} alone (see Sec. IV).

because no one of the three $T_q^{(1-)}(E1-E1)$ and $T_q^{(1-)}(E2-E2)$ or of the seven $T_q^{(3-)}(E2-E2)$ has a polarization dependence of the kind $\epsilon_{\alpha}^* k_{\beta} \epsilon_{\alpha} k_{\beta}$.

Therefore the only allowed terms are time-reversal and parity-odd $E1-E2$ terms. As all four Fe ions belong to equivalent crystallographic positions, it is possible to relate them to one another by means of symmetry operations, in such a way that Eq. (6) can be rewritten as

$$\sigma = (1 + \hat{T}\hat{m}_z)(1 + \hat{T}\hat{C}_{2x})\sigma^{(1)}, \quad (7)$$

where \hat{T} , \hat{m}_z , and \hat{C}_{2x} are, respectively, the operations of time reversal, mirror orthogonal to z , and twofold axis along x . These symmetry operations are intended to act on the $F_q^{(p)}$ tensors. As only time-reversal odd and inversion-odd quantities contribute and as $\hat{m}_z F_q^{(p)} = \hat{I}\hat{C}_{2z} F_q^{(p)} = -(-)^q F_q^{(p)}$ and $\hat{C}_{2x} F_q^{(p)} = (-)^p F_q^{(p)}$,³² we finally get that the only allowed terms are those of the kind: $[1 + (-)^q][F_q^{(p)} - (-)^p F_q^{(p)}]$. Thus, XNDD is sensitive to $F_0^{(1)}$, $F_0^{(3)}$, $F_2^{(2)} - F_{-2}^{(2)}$, and $F_2^{(3)} + F_{-2}^{(3)}$. It is interesting to note that, separately, the first two terms ($F_0^{(1)}$ and $F_0^{(3)}$) were already identified as responsible for the magnetochiral dichroism ($M\chi D$) in Ref. 30, and the second two ($F_2^{(2)} - F_{-2}^{(2)}$ and $F_2^{(3)} + F_{-2}^{(3)}$) for the nonreciprocal gyrotropy (NRG) in Ref. 14. Their contribution to XNDD can be written as follows: $\sigma_b = \sigma_{M\chi D} + \sigma_{NRG}$ and $\sigma_c = \sigma_{M\chi D} - \sigma_{NRG}$, where $\sigma_{M\chi D} \propto -(\sqrt{3}/2\sqrt{5})F_0^{(1)} - (1/\sqrt{10})F_0^{(3)} \equiv \langle t_z - \frac{1}{6}l_z^2 \rangle$ (Ref. 33) and $\sigma_{NRG} \propto 1/\sqrt{6}(F_2^{(2)} - F_{-2}^{(2)}) + (1/\sqrt{3})(F_2^{(3)} + F_{-2}^{(3)}) \equiv \langle (l_x^2 - l_y^2)t_z \rangle - c.c.$ This allows us to disentangle the two contributions as: $\sigma_{M\chi D} = (\sigma_b + \sigma_c)/2$ and $\sigma_{NRG} = (\sigma_b - \sigma_c)/2$. A simple look at the experimental results of Ref. 7 shows that the main con-

tribution comes from σ_{NRG} , as σ_b and σ_c are almost opposite; however $\sigma_{M\chi D}$ is not zero. Notice that the irreducible tensors forming the $M\chi D$ signal both belong to the $\Gamma_4(T_1)$, in Bethe's notation) representation of the cubic group, while those of NRG belong to $\Gamma_5(T_2)$: the former is invariant under \hat{C}_4 rotation, while the latter changes sign, since $l_x^2 \leftrightarrow l_y^2$. This is the reason why they behave differently for b and c dichroism.

Finally, in order to provide a link with the kind of density of states probed by the two dichroisms, we can evaluate the expectation values of $t_z - \frac{1}{6}l_z^2$ and $(l_x^2 - l_y^2)t_z - c.c.$ and find: $\sigma_{M\chi D} \propto d_{xz}^* p_x + d_{yz}^* p_y - c.c.$ and $\sigma_{NRG} \propto d_{xz}^* p_x - d_{yz}^* p_y - c.c.$, where $d_{\alpha\beta}(p_{\alpha})$ are the (complex) coefficients of orbitals of $d_{\alpha\beta}(p_{\alpha})$ type in the wave function. This picture is in complete agreement with the simpler analysis presented in Ref. 7: in fact, from the previous expressions for σ_{NRG} and $\sigma_{M\chi D}$, we get, for b and c -dichroisms, $\sigma_b \propto d_{xz}^* p_x - c.c.$ and $\sigma_c \propto d_{yz}^* p_y - c.c.$, which correspond to the transitions shown in their Fig. 4, mediated by the local polarization and spin orbit, once the change in the axes labels is properly taken into account. Notice, however, that the orbital occupancy amplitude of empty states at pre-edge must be complex, in order to have a magnetic effect (the expectation value of magnetic operators on real orbitals is zero). Remarkably, the temperature dependence reported in Ref. 7, while showing that the XNDD signal follows the temperature profile of the magnetization, provides an indirect proof that polarization does not depend on temperature, as the XNDD signal is linear in the product of polarization and magnetization.

In order to substantiate these considerations, we have performed a numerical simulation with the *ab initio* magnetic code implemented in the fdmnes package.^{19,26} Our results basically confirm the previous picture, as shown in Fig. 2: the order of magnitude of the dichroism, slightly less than 10^{-2} of the absorption, correctly reproduces the experimental data. Moreover, the signal is entirely limited to the pre-edge, at the energy corresponding to the $3d$ density of states, where hybridization of p and d orbitals is stronger: this latter seems to be a general feature of transition metal oxides, as inferred by other similar results.^{11,19,25}

The agreement of our numerical simulation with experimental data, though quite good concerning the above features, is not completely satisfactory regarding the shape of the signal, especially for σ_c dichroism. The reason is probably an overestimation of the $M\chi D$ signal, and is due to the fact that our numerical code is based on a single particle approach and cannot take correctly into account correlation effects, that are undoubtedly strong in such a compound. Similar features were present already in the interpretation of RXS spectra in V_2O_3 .¹⁹ In spite of this, the fact that we are able to determine at least two of the main features of the XNDD signal, like its energy range and the relative magnitude dichroism/absorption, reveal that the main component of such a dichroism, i.e., the NRG part, is determined by the crystal structure, which is correctly taken into account by our independent particle approach.

IV. CONCLUSIONS

In the first part of the paper we give a general classification, based on symmetry arguments, for various kinds of

spectroscopies, in order to relate the corresponding observable quantities with each term of the electromagnetic multipole expansion in the material under study. In particular, we are able to interpret in this way x-ray natural circular dichroism as a measure of the nonmagnetic \tilde{g} -toroidal quadrupole, whereas, in the previous literature,⁶ it was ascribed to the operator $L_z T_z$.

Moreover, we have performed a numerical simulation of the absorption spectra of GaFeO₃ to demonstrate the physical mechanism behind the XNDD. In this respect, a comment is required about the capability of our *ab initio* magnetic code to deal with such tiny effects as the ones determined by parity and time-reversal odd multipoles, even though it is based on a single particle approach. As already stated above, we are able to determine quite well two main features of the XNDD signal, like its energy range and the relative magni-

tude dichroism/absorption. Moreover, as shown in the inset of Fig. 2, the NRG component of the dichroism alone reproduces quite well the experimental signal, which is mainly antisymmetric in the exchange $\sigma_b \leftrightarrow \sigma_c$, with a slight positive offset. Such a positive offset, determined by the $M\chi D$ part of the signal is not well reproduced by our numerical simulation. This seems to imply that the NRG term, roughly determined by the magnetic quadrupole of the system, is well reproduced by our independent particle approach, and, therefore, can be mainly ascribed to an effect of the crystal structure, whereas the $M\chi D$ component of the signal, which depends on the magnetic toroidal moment and octupole, is strongly affected by the electronic correlations and for this reason is badly reproduced by our single particle calculations.

-
- ¹J. D. Jackson, *Classical Electrodynamics* (Wiley, New York, 1975).
- ²V. M. Dubovik and V. V. Tugushev, *Phys. Rep.* **187**, 145 (1990).
- ³Ia. B. Zel'dovich, *Zh. Eksp. Teor. Fiz.* **33**, 1531 (1957) [*Sov. Phys. JETP* **6**, 1184 (1958)].
- ⁴A complete discussion about polar and axial toroidal moments in solid state physics can be found in Ref. 2.
- ⁵C. R. Natoli, Ch. Brouder, Ph. Sainctavit, J. Goulon, Ch. Goulon-Ginet, and A. Rogalev, *Eur. Phys. J. B* **4**, 1 (1998).
- ⁶P. Carra and R. Benoist, *Phys. Rev. B* **62**, R7703 (2000).
- ⁷M. Kubota, T. Arima, Y. Kaneko, J. P. He, X. Z. Yu, and Y. Tokura, *Phys. Rev. Lett.* **92**, 137401 (2004).
- ⁸The magnetic dipole term can be safely neglected in the x-ray range.
- ⁹M. Blume, in *Resonant Anomalous X-Ray Scattering*, edited by G. Materlik, J. Sparks and K. Fisher (Elsevier, Amsterdam, 1994), p. 495.
- ¹⁰P. Carra and B. T. Thole, *Rev. Mod. Phys.* **66**, 1509 (1994).
- ¹¹S. Di Matteo, Y. Joly, A. Bombardi, L. Paolasini, F. de Bergevin, and C. R. Natoli, *Phys. Rev. Lett.* **91**, 257402 (2003).
- ¹²P. Carra, B. T. Thole, M. Altarelli, and X. Wang, *Phys. Rev. Lett.* **70**, 694 (1993).
- ¹³P. Carra, A. Jerez, and I. Marri, *Phys. Rev. B* **67**, 045111 (2003).
- ¹⁴S. Di Matteo and C. R. Natoli, *J. Synchrotron Radiat.* **9**, 9 (2002).
- ¹⁵V. E. Dmitrienko and E. N. Ovchinnikova, *Acta Crystallogr., Sect. A: Found. Crystallogr.* **57**, 642 (2001).
- ¹⁶I. Marri and P. Carra, *Phys. Rev. B* **69**, 113101 (2004).
- ¹⁷B. T. Thole, P. Carra, F. Sette, and G. van der Laan, *Phys. Rev. Lett.* **68**, 1943 (1992).
- ¹⁸For RXS, the presence of the real anomalous term f_j' adds technical complications related to the inversion of Kramers-Krönig relations.
- ¹⁹Y. Joly, S. Di Matteo, and C. R. Natoli, *Phys. Rev. B* **69**, 224401 (2004).
- ²⁰Y. Joly, S. Grenier, and J. E. Lorenzo, *Phys. Rev. B* **68**, 104412 (2003).
- ²¹S. Di Matteo, T. Chatterji, Y. Joly, A. Stunault, J. A. Paixao, R. Suryanaryanan, G. Dhahenne, and A. Revcolevschi, *Phys. Rev. B* **68**, 024414 (2003), and references therein.
- ²²P. Santini and G. Amoretti, *Phys. Rev. Lett.* **85**, 2188 (2000).
- ²³S. W. Lovesey, K. S. Knight, and D. S. Sivia, *Phys. Rev. B* **65**, 224402 (2002).
- ²⁴S. Di Matteo and A. Bombardi (unpublished).
- ²⁵S. Di Matteo, *Phys. Rev. B* **70**, 165115 (2004).
- ²⁶Y. Joly, *Phys. Rev. B* **63**, 125120 (2001). The program can be downloaded at the web address <http://www-cristallo.grenoble.cnrs.fr/simulation>.
- ²⁷J. P. Remeika, *J. Appl. Phys.* **31**, 263S (1960).
- ²⁸The transition temperature depends on the crystal growth, as shown, e.g., in Ref. 31.
- ²⁹G. T. Rado, *Phys. Rev. Lett.* **13**, 335 (1964).
- ³⁰S. Di Matteo and C. R. Natoli, *Phys. Rev. B* **66**, 212413 (2002); see also Ref. 33.
- ³¹T. Arima, D. Higashiyama, Y. Kaneko, J. P. He, T. Goto, S. Miyasaka, T. Kimura, K. Oikawa, T. Kamiyama, R. Kumai, and Y. Tokura, *Phys. Rev. B* **70**, 064426 (2004).
- ³²D. A. Varshalovich, A. N. Moskalev, and V. K. Khersonskii, *Quantum Theory of Angular Momentum* (World Scientific, Singapore, 1988), p. 142, Eqs. (6) and (8).
- ³³Erratum to *Phys. Rev. B* **66**, 212413 (to be published).